Coupled-oscillator model to analyze the interaction between a quartz resonator and trapped ions

E. Altozano,[1] J. Berrocal,[1] S. Lohse,[2,3,4] F. Domínguez,[1] M. Block,[2,3,4] J. J. García-Ripoll,[5] and D. Rodríguez[1,6,*]

[1]*Departamento de Física Atómica, Molecular y Nuclear, Universidad de Granada, 18071 Granada, Spain*

[2]*Department Chemie, Standort TRIGA, Johannes Gutenberg-Universität Mainz, D-55099 Mainz, Germany*

[3]*GSI Helmholtzzentrum für Schwerionenforschung GmbH, D-64291 Darmstadt, Germany*

[4]*Helmholtz-Institut Mainz, D-55099 Mainz, Germany*

[5]*Instituto de Física Fundamental, IFF-CSIC, Serrano 113, 28006 Madrid, Spain*

[6]*Centro de Investigación en Tecnologías de la Información y las Comunicaciones, Universidad de Granada, 18071 Granada, Spain*

(Received 11 July 2022; accepted 9 May 2023; published 30 May 2023)

The novel application of a piezoelectric quartz resonator for the detection of trapped ions has enabled the observation of the quartz-ions interaction under nonequilibrium conditions, opening new perspectives for high-sensitive motional frequency measurements of radioactive particles. Energized quartz crystals have (long) decay-time constants in the order of milliseconds, permitting the coherent detection of charged particles within short time scales. In this paper we develop a detailed model governing the interaction between trapped $^{40}Ca^{+}$ ions and a quartz resonator connected to a low-noise amplifier. We apply this model to experimental data and extract the ions' reduced-cyclotron frequency in our 7-T Penning trap setup. We also obtain an upper limit for the coupling constant g with the present quartz-amplifier-trap (QAT) configuration. The study of the reduced-cyclotron frequency is especially important for the use of this resonator in precision Penning-trap mass spectrometry. The improvement in sensitivity can be accomplished by increasing the quality factor of the QAT configuration, which in turn will improve the performance of the system towards the strong-coupling regime.

DOI: 10.1103/PhysRevA.107.053116

I. INTRODUCTION

Electronic detection of trapped charged particles in Penning traps is used in a variety of experiments in fundamental physics [1,2] as well as for applications in chemistry and biology [3]. Most of these experiments pertain to mass spectrometry aiming at reaching the highest precision when only a single ion [4] or an ion pair [5] is in the Penning trap, or when the highest precision is not required, aiming at identifying molecules using tens of ions or more from the same species without frequency-selective amplification. The increase in sensitivity to reach single-ion detection relies mainly on the use of high-Q resonators, which until very recently were made mostly of superconducting solenoids [6,7]. Recent developments in Penning trap experiments have demonstrated that quartz crystals can serve as resonators, covering, depending on the cut along the crystallographic axis of the crystal, different frequency regimes, from MHz (AT cut) [8] to a few hundred kHz (SL cut) [9]. The latter work includes the first proof of a cyclotron-frequency ratio measurement of two ion species. Quartz resonators benefit from a relatively long decay-time constant of a few milliseconds when the quartz is energized by a resonant radio-frequency (rf) field. This has resulted in the observation of the coherent interaction between the resonator and trapped ions under nonequilibrium conditions, without the need for long observation times. This has been presented in a recent work [10] opening prospects for nondestructive detection of exotic nuclei at existing facilities [11,12] or facilities under construction [13]. Two models were introduced in Ref. [10], one based on the ions' equivalent circuit [14], which is the one applied in precision Penning-trap mass spectrometry [15], and the other based on the coupling between the quartz and ions considering each system as a harmonic oscillator. In this paper we have fully developed the coupled-oscillators model using the experimental data presented in Ref. [10]. An analysis procedure has been established, which allows us to extract precise motional frequency values from the quartz-ion interaction at different times after the ions and the crystal have been energized. Important parameters for the applicability of the system are the coupling constant and the ions' reduced-cyclotron frequency. A high precision in the determination of the latter might allow using this system for Penning-trap mass spectrometry on a single ion, a field exploited so far with stable ions, in the domain of superconducting-solenoid based detection setups [1,2,4]. This approach calls for single-ion sensitivity. Due to the range of frequencies available, another application in the field of Penning-trap mass spectrometry will be the coupling of ions in physically separated traps [16]. This will allow using fluorescence photons from a laser-cooled $^{40}Ca^{+}$ (sensor) ion to weigh heavy nuclei [17], extending what has been done for the cooling of protons via a cloud of laser-cooled $^{9}Be^{+}$ ions when connecting the two traps to an LC circuit [18]. Such coupling, and the unique feature of operation under nonequilibrium, might extend the use of quartz crystals and the model presented here beyond mass spectrometry with further exploitation of the hybrid system quartz ion for quantum applications [19].

*danielrodriguez@ugr.es

II. PENNING TRAP AND INDUCED IMAGE CURRENT

In a Penning trap an ion with mass m_{ion} and charge q_{ion} is confined by the superposition of an electrostatic quadrupole field with a strong homogeneous magnetic field [20]. The latter defines the revolution-symmetry axis ($\vec{B} = B\,\vec{e}_z$) of the device made in the simplest configuration by a ring electrode and two endcaps. The configuration of the electrodes is such that the electrostatic potential inside the trap volume, when a voltage U_0 is applied between the ring and endcap electrodes, is given by

$$V(x,\ y,\ z) = \frac{U_0}{4d^2}(-x^2 - y^2 + 2z^2), \tag{1}$$

where $d = \frac{1}{2}\sqrt{2z_0^2 + d_0^2}$ and z_0 and d_0 are the distances from the trap center to the endcap and ring electrode, respectively. The ion motion due to the Lorentz force acting on it can be depicted as the superposition of three eigenmotions, one in the axial direction with a characteristic frequency

$$\omega_z = \sqrt{\frac{q_{\text{ion}}U_0}{m_{\text{ion}}d^2}}, \tag{2}$$

and two in the radial plane with characteristic frequencies

$$\omega_\pm = \tfrac{1}{2}\left(\omega_c \pm \sqrt{\omega_c^2 - 2\omega_z^2}\right) \tag{3}$$

where

$$\omega_c = \frac{q_{\text{ion}}B}{m_{\text{ion}}} \tag{4}$$

is the cyclotron frequency of the ion. The subscripts $+$ and $-$ in Eq. (3) represent the modified-cyclotron and magnetron motion, respectively. The quantum Hamiltonian is presented in Appendix A.

The reduced-cyclotron frequency can be measured if an electrode is used as pick-up current detector, since this current is modulated by the ion motion. Our experiments are focused on the detection of ω_+, and thus the radial motion in the $x - y$ plane has to be considered. In a first-order approximation of the radial motion, the charge induced on the detection segment (DS in Fig. 1) by a trapped ion only depends on x (following the nomenclature in Fig. 1) as

$$Q_{\text{ion}}(x, y) \approx Q_{\text{ion}}(x,\ 0) \approx -\frac{q_{\text{ion}}\alpha}{2}\left(1 + \frac{x}{d_0}\right), \tag{5}$$

where α is a geometrical factor that accounts for the deviation of the geometry of the trap electrodes from the ideal case of two parallel plates, and d_0 is depicted in Fig. 1. The induced image current is given by

$$I_{\text{ion}}(p_x,\ p_y) \approx I_{\text{ion}}(p_x, 0) \approx -\frac{q_{\text{ion}}\alpha}{2d_0 m_{\text{ion}}}p_x. \tag{6}$$

III. THE QUARTZ-ION COUPLED-OSCILLATOR MODEL

The full system is depicted in Fig. 2 and the associated Hamiltonian comprises the following contributions:

$$H_{\text{total}} = H_{\text{ion}} + H_{\text{q}} + H_{\text{int}} + H_{\text{rf}} \tag{7}$$

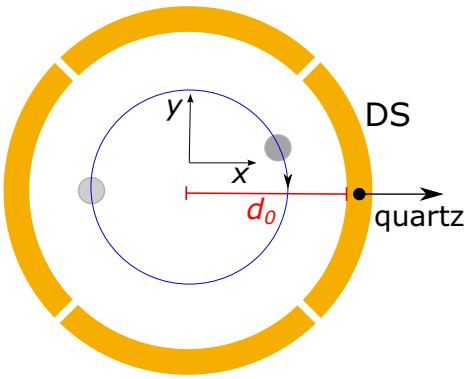

FIG. 1. Transverse cut of a ring electrode in a Penning trap with cylindrical symmetry. The electrode is divided in four segments. The ions' trajectory in the radial plane, considering only modified-cyclotron motion for illustration purposes, is depicted by the blue-solid line. The light and dark-gray solid circles represent the trapped ions when they are far or close, respectively, to the detection segment (DS) where the current they induce is picked up. DS is connected to the quartz resonator followed by an amplifier [8].

where H_{q} denotes the dynamics of the quartz crystal, H_{ion} denotes that of the trapped ions, H_{int} denotes the interaction between the quartz and the ions, and H_{rf} denotes the interaction of each one with an external rf driving field. All these terms will be described in the following, giving them as a function of the creation and annihilation operators $a^\dagger$ and a, for the ions, and $b^\dagger$ and b for the quartz.

The Hamiltonian describing the ion motion in a Penning trap is presented in Appendix A1. Since only the modified-cyclotron motion is in resonance with the quartz, one can write

$$H_{\text{ion}} \approx \hbar\omega_+\left(a_+^\dagger a_+ + \tfrac{1}{2}\right) \equiv \hbar\omega_{\text{ion}}\left(a^\dagger a + \tfrac{1}{2}\right) \tag{8}$$

and $\langle a\rangle \equiv |\langle a\rangle|e^{i\theta_a}$.

The Hamiltonian describing the quartz is given by

$$H_{\text{q}} = \left(\frac{k}{C_{\text{q}}}\right)^2\left(\frac{m_{\text{q}}}{2}\hat{I}^2 + \frac{m_{\text{q}}\omega_{\text{q}}^2}{2}\hat{Q}^2\right) = \hbar\omega_{\text{q}}\left(b^\dagger b + \frac{1}{2}\right), \tag{9}$$

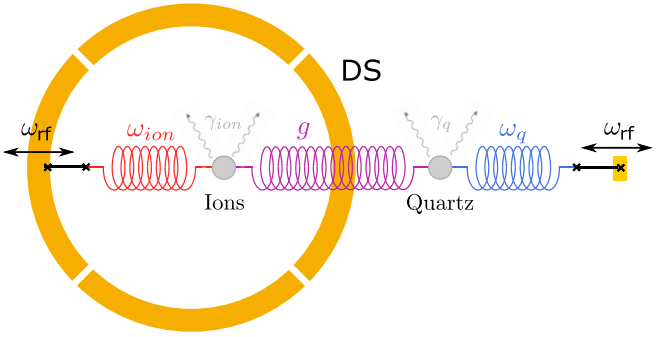

FIG. 2. Schematic view of the quartz-ion coupled-oscillators model. The external (rf) voltage is applied to the electrode on the left.

with

$$b = \frac{k}{C_q}\sqrt{\frac{m_q\omega_q}{2\hbar}}\left[\hat{Q} + \frac{i}{\omega_q}\hat{I}\right] \tag{10}$$

and $\langle b\rangle \equiv |\langle b\rangle| e^{i\theta_b}$ its expected value. The operators $\hat{Q}$ and $\hat{I}$ related to charge and current, respectively, are defined in Appendix A2. We model the crystal as a cylindrical shape of length l and consider the vibration to be in the axial direction. k is a proportionality constant which relates the expansion of the piezoelectric crystal Δl with the applied voltage V, C_q is the capacitance of the quartz resonator (Q/V), and m_q the mass of the quartz's oscillation mode with eigenfrequency ω_q.

Following Appendix A3, and considering that the magnetron motion is not in resonance, the Hamiltonian describing the quartz-ion interaction can be written as

$$\begin{aligned} H_{\text{int}} &= \left(\frac{k}{C_q}\right)^2\left(-\frac{\xi N_{\text{ion}} q_{\text{ion}}\alpha m_q}{2d_0 m_{\text{ion}}}\hat{I}\hat{p}_x - \frac{\xi N_{\text{ion}} q_{\text{ion}}\alpha m_q\omega_q^2}{2d_0}\hat{Q}\hat{x}\right) \\ &\approx \hbar g a^\dagger b + \hbar g^* b^\dagger a, \end{aligned} \tag{11}$$

where N_{ion} is the number of trapped ions and $g/2\pi$ represents the coupling constant in Hz. Taking into account that $\omega_- \ll \omega_+$ and $\omega_q \approx \omega_+$, the coupling constant can be written as

$$\begin{aligned} g &= i\frac{k}{C_q}\frac{\xi q_{\text{ion}}\alpha(\omega_q + 2\omega_-)}{4d_0}\sqrt{\frac{N_{\text{ion}} m_q\omega_q}{m_{\text{ion}}(\omega_+ - \omega_-)}} \\ &\approx i\frac{k}{C_q}\frac{\xi q_{\text{ion}}\alpha\omega_{\text{ion}}}{4d_0}\sqrt{\frac{N_{\text{ion}} m_q}{m_{\text{ion}}}}. \end{aligned} \tag{12}$$

The Hamiltonian describing the interaction between the ions and quartz crystal with an external rf field reads

$$\begin{aligned} H_{\text{rf}} = &\frac{F_{\text{ion}}}{\sqrt{2}}\cos(\omega_{\text{rf}}t + \phi_{\text{ion}})(a + a^\dagger) \\ &+ \frac{F_q}{\sqrt{2}}\cos(\omega_{\text{rf}}t + \phi_q)(b + b^\dagger), \end{aligned} \tag{13}$$

where ω_{rf} is the frequency of the field, F_{ion} and F_q are the amplitudes of the forces exerted on the ions and on the quartz, respectively, and ϕ_{ion} and ϕ_q are their phases.

Working in the Heisenberg picture, the operators a and b oscillate with frequencies $e^{-i\omega_{\text{ion}}t}$ and $e^{-i\omega_q t}$, respectively. Using the rotating wave approximation we find that

$$\frac{F_{\text{ion}}}{\sqrt{2}}\cos(\omega_{\text{rf}}t + \phi_{\text{ion}})(a + a^\dagger) \sim + \frac{F_{\text{ion}}}{\sqrt{2}}(e^{i(\omega_{\text{rf}}t + \phi_{\text{ion}})}a + \text{H.c.}), \tag{14}$$

and

$$\begin{aligned} H_{\text{total}} = &\hbar\tilde{\omega}_{\text{ion}} a^\dagger a + \hbar\tilde{\omega}_q b^\dagger b + \hbar g a^\dagger b + \hbar g^* b^\dagger a \\ &+ \hbar f_{\text{ion}}(e^{i\phi_{\text{ion}}}a + \text{H.c}) + \hbar f_q(e^{i\phi_q}b + \text{H.c.}) \end{aligned} \tag{15}$$

where $\tilde{\omega}_{\text{ion}} = \omega_{\text{ion}} - \omega_{\text{rf}}$ and $\tilde{\omega}_q = \omega_q - \omega_{\text{rf}}$, and the effective forces $f_{\text{ion}} = \frac{\hbar}{\sqrt{2}}F_{\text{ion}}$ and $f_q = \frac{\hbar}{\sqrt{2}}F_q$.

The fundamental model that governs the evolution of the hybrid quartz-ion system is a master equation of two coupled oscillators under finite-temperature baths,

$$i\frac{d}{dt}\rho = -\frac{i}{\hbar}[H_{\text{total}}, \rho] + \mathcal{L}(\rho) = \mathcal{L}_{\text{tot}}(\rho, t), \tag{16}$$

which includes the coherent interaction [Eq. (7)] and a heating term:

$$\begin{aligned} \mathcal{L}(\rho) = &\gamma_q n_q\left(b^\dagger\rho b - \frac{1}{2}bb^\dagger\rho - \frac{1}{2}\rho bb^\dagger\right) \\ &+ \gamma_q(n_q + 1)\left(b\rho b^\dagger - \frac{1}{2}b^\dagger b\rho - \frac{1}{2}\rho b^\dagger b\right) \\ &+ \gamma_{\text{ion}} n_{\text{ion}}\left(a^\dagger\rho a - \frac{1}{2}aa^\dagger\rho - \frac{1}{2}\rho aa^\dagger\right) \\ &+ \gamma_{\text{ion}}(n_{\text{ion}} + 1)\left(a\rho a^\dagger - \frac{1}{2}a^\dagger a\rho - \frac{1}{2}\rho a^\dagger a\right), \end{aligned} \tag{17}$$

where

$$n_q = \frac{1}{e^{\hbar\omega_q/k_B T_q} - 1} \approx \frac{k_B T_q}{\hbar\omega_q} \tag{18}$$

is the phonon number in the thermal bath of the quartz and γ_q is a dissipative constant to account for the interaction with this environment. γ_q is related to the quality factor Q of the resonator by $\gamma_q = \omega_q/Q$. Likewise, n_{ion} is the number of phonons in the thermal bath of the ions, and γ_{ion} is the dissipative constant of the ion cloud due to phenomena not described by H_{total}, e.g., internal degrees of freedom in the cloud, interaction with different electrodes, or collisions with residual-gas atoms or molecules.

IV. EXPERIMENTAL SIGNAL COMPUTATION

The master equation (16) is linear. We can therefore write formally its solution for an initial condition $\rho(t_0)$ as a positive map $\rho(t) = \varepsilon[\rho(t_0), t, t_0]$ with some expression $\varepsilon[\cdot]$ to be determined. In absence of the external driving field, with a time-independent Lindblad operator $\mathcal{L}_{\text{tot}}$, the positive map is independent of the initial condition and only depends on the time interval that we investigate:

$$\rho(t) = e^{t\mathcal{L}_{\text{tot}}}\rho(0) = \varepsilon_t[\rho(t_0)]. \tag{19}$$

The system evolves following Eq. (16) for a certain time; then the voltage on the quartz oscillator, $V_i(t)$, is measured for sequential times t. This list of voltage traces is Fourier transformed for every measurement iteration i:

$$\tilde{V}_i(\omega; t_0, t_1) = \frac{1}{\sqrt{t_1 - t_0}}\int_{t_0}^{t_1} e^{-i\omega t}V_i(t)dt. \tag{20}$$

The analyzed experimental signal, the power spectral density (PSD), is approximated by the average of these quantities, over a number of measurements N, as

$$S(\omega; t_0, t_1, N) := \frac{1}{N}\sum_{i=1}^{N}|\tilde{V}_i(\omega; t_0, t_1)|^2. \tag{21}$$

This can be related to any quantum observable in the combined quartz-ion system. From the original time traces

$$S(\omega; t_0, t_1, N) = \int_{t_0}^{t_1}\int_{t_0}^{t_1} d\tau_1 d\tau_2 e^{i\omega(\tau_1-\tau_2)} \sum_{i=1}^{N} \frac{V_i(\tau_1)V_i(\tau_2)}{t_d N}, \tag{22}$$

where $t_d = t_1 - t_0$ is the duration of the integrated signal. In the limit of a large number of measurements $N \to \infty$, this estimator approximates the PSD evaluated over the initial quantum state:

$$S(\omega; t_0, t_1) := \frac{1}{t_d}\int_{t_0}^{t_1}\int_{t_0}^{t_1} d\tau_1 d\tau_2 e^{i\omega(\tau_1-\tau_2)} \langle \hat{V}(\tau_2)\hat{V}(\tau_1)\rangle . \tag{23}$$

In the limit of infinite time t_d and stationary systems, this quantity approaches the usual definition of power spectral density [21]:

$$\lim_{t_d\to\infty} S(\omega; t_0, t_1) := \int_{-\infty}^{\infty} e^{-i\omega\tau} \langle \hat{V}(\tau)\hat{V}(0)\rangle . \tag{24}$$

In order to match the experiments and the theory, one needs to compute two-time correlators $\langle \hat{V}(t_1)\hat{V}(t_2)\rangle$ for the quartz-ion system. This will be approached in a slightly more general way, and the correlators $\langle A_n(t)A_m(t')\rangle$ will be computed for a collection of Fock operators that form a suitable basis for all the observables of interest:

$$\mathbf{A} = \begin{pmatrix} a \\ b \\ a^\dagger \\ b^\dagger \end{pmatrix}. \tag{25}$$

Using these operators, one can reconstruct the observables of interest:

$$\hat{V} = V_0 \frac{1}{\sqrt{2}}(b + b^\dagger) \equiv \mathbf{v}^{\mathrm{T}} \cdot \mathbf{A}. \tag{26}$$

In these canonical coordinates, we recover the PSD

$$S(\omega; t_0, t_1) = \mathrm{Re} \sum_{m,n} v_m v_n S_{mn}(\omega), \tag{27}$$

from a slightly more general PSD matrix:

$$S_{mn}(\omega; t_0, t_1) := \int_{t_0}^{t_1}\int_{t_0}^{t_1} d\tau_1 d\tau_2 \frac{e^{i\omega(\tau_1-\tau_2)}}{t_d} \langle A_m(\tau_2)A_n(\tau_1)\rangle . \tag{28}$$

Our approach to compute the PSD involves three steps. The first step is to recover the **A** operators while the ion and the quartz are driven. This allows us to obtain the initial conditions for the spectroscopy experiment, right at the time $t = 0$ where the driving field is switched off. The second step is to solve the correlators during the spectroscopy phase, so that we can gather the statistics of the voltage traces from t_0 up to $t_1 = t_0 + t_d$. The third step is to Fourier transform the resulting correlators to recover Eq. (23).

Power spectral density computation

As shown in Appendix B the PSD can be written as the sum of two terms, a thermal noise plus the coherent signal that results from the damped oscillations in both the quartz resonator and the ions [Eq. (B19)]. One can also add a frequency independent term arising from the electronic noise of the circuit, so that the total power can be written as the sum of three terms:

$$S(\omega) = S^{\mathrm{coh}}(\omega) + S^{\mathrm{th}}(\omega) + S^{\mathrm{noise}}. \tag{29}$$

The coherent part of the PSD may be derived from the dynamics of the first-order moments:

$$S^{\mathrm{coh}}(\omega; t_0, t_1)_{mn} = \tilde{A}_m(\omega; t_0, t_1)\tilde{A}_n(-\omega; t_0, t_1), \tag{30}$$

where

$$\tilde{A}_m(\omega; t_0, t_1) = \frac{1}{\sqrt{t_d}}\int_{t_0}^{t_1} e^{-i\omega t} \langle A_m(t)\rangle \, dt \tag{31}$$

is the Fourier transform of the first-order moments. Given the exact dynamics for the first-order moments (B11), these integrals can be computed (see Appendix B4), obtaining

$$\tilde{\mathbf{A}} = (-i\omega - \mathbf{M})^{-1}[e^{-i\omega t_d} \langle \mathbf{A}(t_1)\rangle - \langle \mathbf{A}(t_0)\rangle]. \tag{32}$$

The voltage PSD is the sum of four terms in the S_{mn} matrix:

$$S^{\mathrm{coh}}(\omega; t_0, t_0 + t_d) = \frac{V_0^2}{2t_d}[\tilde{A}_2(\omega) + \tilde{A}_4(\omega)][\tilde{A}_2(-\omega) + \tilde{A}_4(-\omega)]. \tag{33}$$

This can be simplified, due to the organization of the $\tilde{\mathbf{A}}$ vector, $\tilde{A}_4(\omega) = \tilde{A}_2(-\omega)^*$. In addition, for $\omega > 0$, only the lower-right sector of the inverse of $(-i\omega - \mathbf{M})$ [Eq. (B26)] survives, hence $\tilde{A}_4(-\omega) = \tilde{A}_2(\omega)^* \simeq 0$ whenever $\omega > 0$. Thus

$$S^{\mathrm{coh}}(\omega; t_0, t_0 + t_d) = \frac{V_0^2}{2t_d}|\tilde{A}_4(\omega)|^2, \tag{34}$$

where

$$\tilde{A}_4(\omega) = -F(\omega)^* i g \Big\{ [e^{-i\omega t_d} \langle a^\dagger(t_1)\rangle - \langle a^\dagger(t_0)\rangle] + \left[i(\omega - \omega_{\mathrm{ion}}) + \frac{\gamma_{\mathrm{ion}}}{2} \right][e^{-i\omega t_d} \langle b^\dagger(t_1)\rangle - \langle b^\dagger(t_0)\rangle] \Big\}, \tag{35}$$

with the envelope

$$F(\omega)^* = \frac{1}{\left[i(\omega - \omega_{\mathrm{ion}}) + \frac{\gamma_{\mathrm{ion}}}{2}\right]\left[i(\omega - \omega_{\mathrm{q}}) + \frac{\gamma_{\mathrm{q}}}{2}\right] + |g|^2}. \tag{36}$$

The thermal component of the PSD can be written as the real part of a single matrix integral (see Appendix B5):

$$S^{\mathrm{th}}(\omega) = 2\mathrm{Re} \sum_{mn} v_m v_n S^+_{mn}(\omega), \text{ with} \tag{37}$$

$$S^+_{mn}(\omega) = \frac{1}{t_d}\sum_r \int_{t_0}^{t_1} dt \int_0^{t_d - t} d\tau e^{-i\omega\tau} U_{mr}(\tau) \langle A_r A_n\rangle_{\mathrm{th}} . \tag{38}$$

Since the expectation value inside the integral is constant, one only needs to compute the matrix:

$$\begin{aligned}\mathbf{Q}(\omega) &= \frac{1}{t_d}\int_0^{t_d} dt \int_0^{t_d - t} d\tau e^{(-i\omega - \mathbf{M})\tau} \\ &= \frac{1}{t_d}(-i\omega - \mathbf{M})^{-2}(e^{(-i\omega-\mathbf{M})t_d} - \mathbb{1}) \\ &\quad + (-i\omega - \mathbf{M})^{-1}\frac{1}{t_d} \times t_d \\ &\simeq (-i\omega - \mathbf{M})^{-1} \text{ as } t_d \to +\infty. \end{aligned} \tag{39}$$

Given this simplification in the limit of long integration times, the thermal PSD is

$$S^{+}_{mn}(\omega) = 2[(-i\omega - \mathbf{M})^{-1}\mathbf{T}]_{mn} \tag{40}$$

with the matrix of static correlations from Eq. (B36). Since $\mathbf{T}$ is only nonzero in two sectors, and since we know the explicit expressions for the inverse of $\mathbf{M}$, one can write

$$\mathbf{S}^{+}(\omega) \simeq \begin{pmatrix} 0 & F(-\omega)\mathbf{G}(-\omega)\mathbf{t}_{-\dagger} \\ F(\omega)^{*}\mathbf{G}(\omega)^{*}\mathbf{t}_{-\dagger} & 0 \end{pmatrix}. \tag{41}$$

As before, $F(-\omega) \simeq 0$ for positive values of ω. Out of this mostly zero matrix, only one element contributes to the autocorrelation of the potential and the thermal PSD is

$$S^{\text{th}}(\omega) = \frac{V_0^2}{2} \times 2\text{Re}[S^{+}_{b^\dagger b}(\omega)]. \tag{42}$$

Introducing the explicit formula for $\mathbf{G}(\omega)$, one obtains

$$S^{+}_{bb^\dagger}(\omega) = F(\omega)^{*}\left\{ig\,\langle a^\dagger b\rangle_{\text{th}} + \left[\frac{\gamma_{\text{ion}}}{2} + i(\omega - \omega_{\text{ion}})\right]\langle b^\dagger b\rangle_{\text{th}}\right\}, \tag{43}$$

where $\langle a^\dagger b\rangle_{\text{th}}$ and $\langle b^\dagger b\rangle_{\text{th}}$ are given in Appendix B6.

V. RESULTS AND DISCUSSION

The fit to the experimental data is done with $S(\omega)$ [Eq. (29)]. Zero padding has been applied to our experimental data, i.e., a list of equidistant zeros has been added after time t_1 until reaching 20 s to improve the resolution of the frequency spectrum [9]. The terms accounting for the coherent and thermal interaction, named as $S^{\text{coh}}(\omega)$ and $S^{\text{th}}(\omega)$, respectively, are shown in Eqs. (34) and (42). Many parameters have to be considered: S^{noise}, γ_{ion}, γ_{q}, ν_{ion}, ν_{q}, $|g|$, n_{ion}, n_{q}, $|\langle a\rangle|$, $|\langle b\rangle|$, θ_a, θ_b, f_{ion}, f_{q}, ϕ_{ion}, and ϕ_{q}. We consider $\theta_{\text{b}} = 0$ because it can be factored out as a global phase and neglected due to the absolute value in $S^{\text{coh}}(\omega)$. Under this assumption, only the relative phase $\delta \sim \theta_{\text{a}}$ is relevant for the fit. To simplify the analysis, we only consider $t_0 \geqslant 0$, to neglect the rf field related terms f_{ion}, f_{q}, ϕ_{ion}, and ϕ_{q}. A full fitting procedure consists of three steps described in the following.

(1) Fit of the background signal $S^{\text{th}}(\omega) + S^{\text{noise}}$ (without ions) using Eq. (42) with $|g| = 0$. This will yield the parameters n_{q}, γ_{q}, and S^{noise}. It will also yield ν_{q} although this will be considered as free parameter later. The left panel of Fig. 3 shows the evolution of $n_{\text{q}}V_0^2$ and S^{noise} for times t_0 in which the quartz is completely thermalized. The right panel shows the results for γ_{q}.

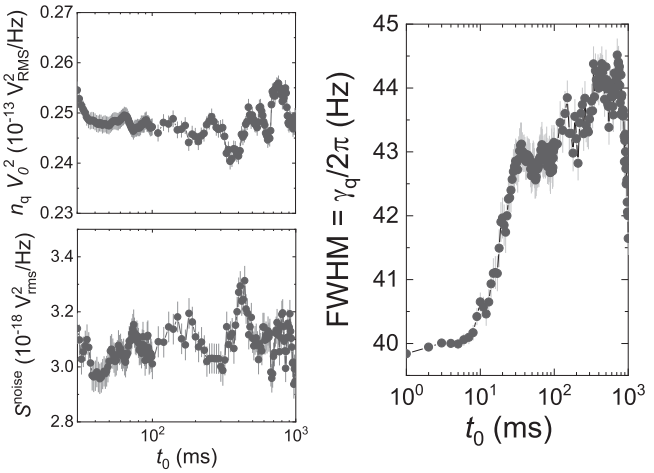

FIG. 3. Left panel: $n_{\text{q}}V_0^2$ (top) and S^{noise} (bottom) as a function of the time t_0. Right panel: FWHM $\equiv \gamma_{\text{q}}/2\pi$ as a function of the time t_0.

(2) Fit of the full signal $S(\omega, t_0)$ (with ions) for a fixed frequency value $\omega_1 = 2\pi\nu_1$, as a function of t_0, thus moving the integration window and taking $\gamma_{\text{ion}} = 0$, to obtain $|g| \approx 2\pi \times 1.45$ Hz. $t_0 = 0$ is the time when the rf driving field is stopped. We consider $n_{\text{ion}} = n_{\text{q}}$ since in equilibrium the resonator is at room temperature and its interaction with the ions is done through the detection electrode also at room temperature. Further details are given in Appendix C.

(3) Fit of the full signal $S(\omega)$ (with ions) considering as fixed parameters γ_{q}, γ_{ion}, $n_{\text{q}} = n_{\text{ion}}$, and $|g|$. Five parameters are obtained from the fit: δ, ν_{ion}, ν_{q}, $|\langle a(t_0)\rangle|$, and $|\langle b(t_0)\rangle|$.

The data points for about $N_{\text{ion}} = 6000$ [10] and the fits for $t_0 = 0$ are shown in Fig. 4. Results considering other values of t_0 are presented in Fig. 5. The data acquisition window t_d considered for the fits is always 1 s, which is a reasonable compromise between a high frequency

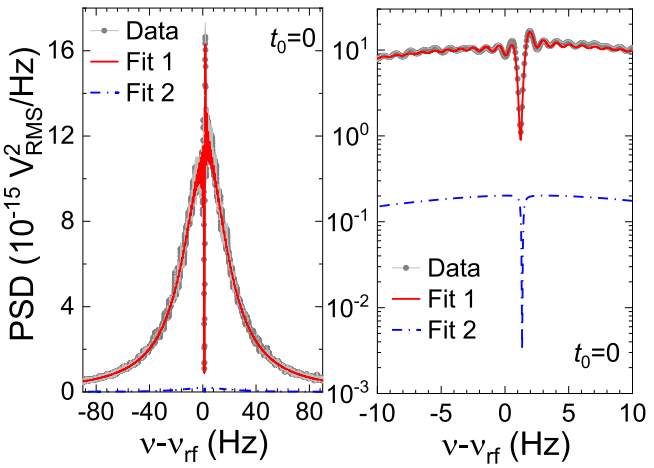

FIG. 4. PSD signal as a function of the frequency for $t_0 = 0$ ms. A zoomed plot is shown in the right panel. The red-solid line in both panels (fit 1) is the $S(\omega)$ fit. The blue-dashed-dotted line (fit 2) is the $S^{\text{th}}(\omega) + S^{\text{noise}}$ fit. $\chi^2_\nu = 1.18$. The data points and standard deviations (1 σ) are the results from $N = 20$ measurements.

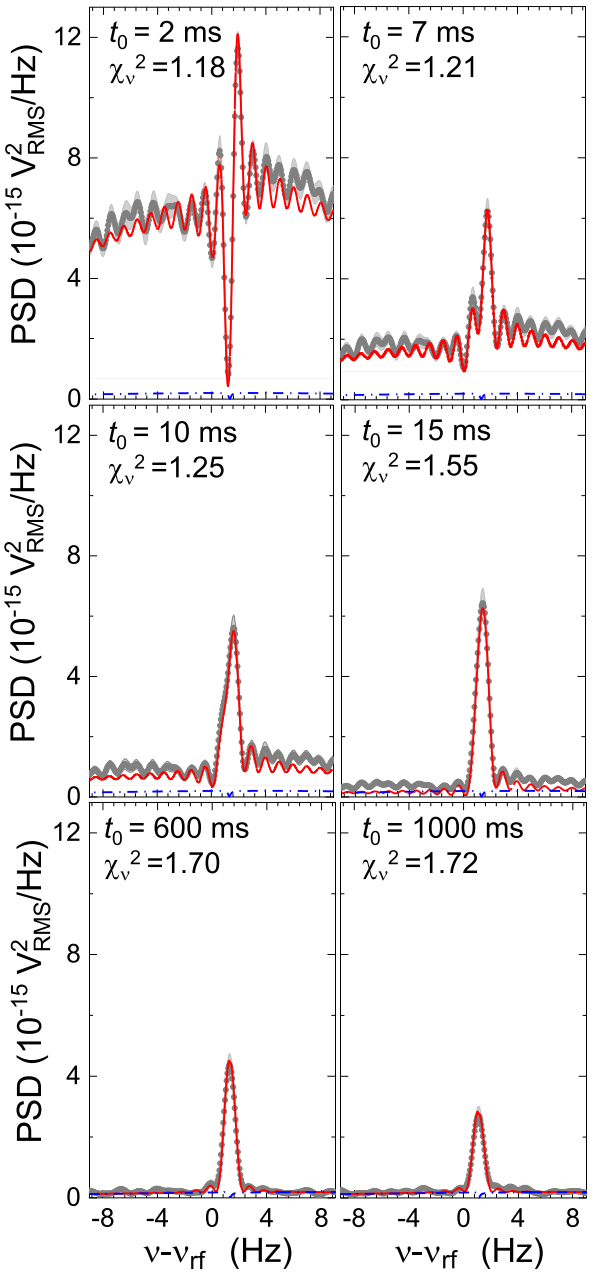

FIG. 5. Evolution of the PSD signal and fitting function for different times t_0. The data points and standard deviations are the results from $N = 20$ measurements.

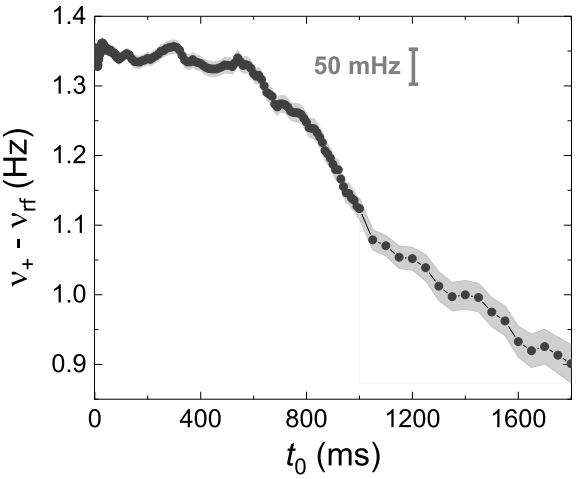

FIG. 6. Evolution of ν_{ion} obtained from the fit using Eq. (29) as a function of t_0. The vertical line covers 50 mHz.

resolution and short acquisition times. For $t_d \gtrsim 2$ s the fit function $S(\omega)$ does not converge since ν_{ion} is not stable after some hundreds of milliseconds (see below). The effective relative phase (ERP) between quartz and trapped ions, which is defined as $\text{ERP} \equiv \pi/2 - \arg\{g\} - \delta(t_0)$, because of the $ig^*\langle a^\dagger(t_0)\rangle = e^{i(\pi/2-\arg\{g\}-\delta(t_0))}|g||\langle a^\dagger(t_0)\rangle| \equiv e^{i\cdot\text{ERP}}|g||\langle a^\dagger(t_0)\rangle|$ factor in Eq. (35), is $\approx 150^o$ for t_0 varying from 0 to 25 ms. For $t_0 > 25$ ms, the ERP decreases gradually down to 0^o at $t_0 \approx 50$ ms. The different phase implies the subtraction or sum of the Lorentzian functions quantified in Eq. (35). This gives rise to a dip or a peak signal. The dip is only visible while the crystal is still energized after the driving.

The use of quartz crystals for high-precision Penning-trap mass spectrometry relies on how accurately motional frequencies can be determined. A final statement on the accuracy can be made if single-ion sensitivity is reached. The discussion here is limited to the improvement in precision observed by applying this model. Figure 6 shows the evolution of $\nu_{ion} \equiv \nu_+$ as a function of t_0. The analysis procedure developed in this paper results in a precise value when t_0 is varied from 0 to 600 ms, improving the results based on Gaussian fits presented in Ref. [10]. Using the coupled-oscillators model, the standard deviation in the range $t_0 = 0$–15 ms is reduced by a factor of 6 compared to the result obtained from the Gaussian fits in the previous work. Furthermore, the standard deviation considering the time range from 0 to 600 ms is only 10 mHz. The trend in the frequency towards lower values observed in Fig. 6 might be assigned to the different motional amplitude of the ions due to the interaction with the energized or room-temperature quartz. This temperature difference can be only accounted for if the coefficients to quantify the anharmonicities due to electric-field imperfections are known, and one can take as reference the value of ν_+ from a measurement on a single ion with the lowest motional amplitudes.

Finally, the case where ν_{ion} is shifted from ν_q is outlined. Figure 7 shows the PSD signal as a function of the frequency for two different values of t_0. For these data, the amplitude of the rf field was a factor of 16 larger, compared to the data shown in Figs. 4 and 5. This is because here the ions were previously laser cooled. A total of 750 ions were trapped [10]. For the presentation of these data, the analysis procedure has been shortened, considering the γ_q variable and using $|g|$ (scaled with the number of ions) obtained from the first set of data. Thus, the second step, which is presented in Appendix C, has been omitted.

VI. CONCLUSIONS AND OUTLOOK

In this paper we have demonstrated that the hybrid system quartz-trapped ions behaves as a coupled-oscillators system.

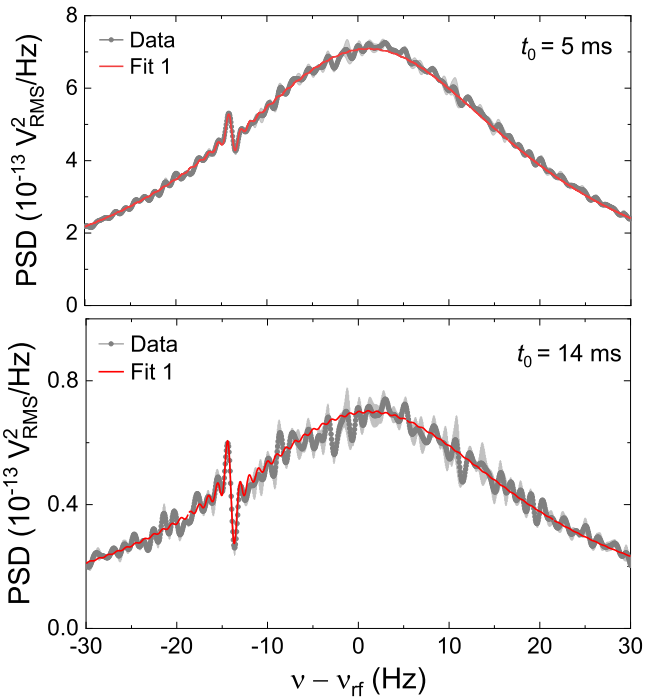

FIG. 7. PSD signals as a function of the frequency for $t_0 = 5$ ms (top) and $t_0 = 14$ ms (bottom). The red-solid line (fit 1) is the $S(\omega)$ fit. The $S^{\text{th}}(\omega)$ fit is not shown since it is not visible in this scale. Note that the PSD is two orders of magnitude larger compared to Fig. 4 because the rf field amplitude applied here is 16 times larger. The data points and standard deviations are the results from three measurements.

The fitting function to analyze the experimental PSD obtained for the charge induced by an ion cloud on trap electrodes has been fully developed. The evolution of the ions' signal from a dip to a peak structure is explained due to a change in the relative phase between the two oscillators and the change in amplitude of the Lorentzian function used to describe the response of the quartz crystal. From the analysis procedure, we obtain the modified-cyclotron frequency, and the first motivation for our research, i.e., mass spectrometry, has been discussed. Here, an increase in sensitivity is mandatory, and can be achieved by increasing the quality factor of the system and reducing its temperature of operation. In the experiments reported here, the quality factor Q of the quartz crystal varied from 66 800 to 60 700 depending on the energy stored in the crystal. Very recently, we have improved the quality factor of the QAT system by a factor of ≈2. Further improvements are anticipated since the measured quality factor of the bare QA system is a factor of ≈500 larger.

Another important parameter has been obtained, namely, the ions-quartz coupling constant. This has been determined following the procedure described in Appendix C, to be as large as $|g| \approx 2\pi \times 1.45$ Hz from our data with the present configuration. From Eq. (12), it is possible to increase g by reducing the distance between electrodes, by modifying the trap geometry quantified by α, by increasing N_{ion} or ω_+, or by increasing ξ. Note that the latter includes the parameters such as parasitic capacitances, or electronic noise, that diminish the sensitivity. Increasing ξ will allow increasing Q and the sensitivity using the same Penning trap and $^{40}Ca^+$. An increase of α requires a different trap geometry. Larger values of ω_+ are possible using highly charged ions. An increase of g and Q, and the operation of the system at very low temperature, might be first used to accelerate the interaction of ions stored in different traps following the original proposal by Heinzen and Wineland [16]. Applications beyond mass spectrometry or sympathetic cooling, i.e., applications in the strong-coupling regime, will require $^{40}Ca^+$, a coupling constant of a few kHz, and a Q value in the order of 10^8.

ACKNOWLEDGMENTS

We acknowledge support from the Spanish MCINN through Project No. PID2019-104093GB-I00/AEI/10.13039/501100011033 and Contract No. PTA2018-016573-I, and from the Andalusian Government through Project No. P18-FR-3432 and Fondo Operativo FEDER Grant No. A-FQM-425-UGR18, from the Spanish Ministry of Education through Ph.D. fellowship Grant No. FPU17/02596, and from the University of Granada "Plan propio—Programa de Intensificación de la Investigación," Project No. PP2017-PRI.I-04 and "Laboratorios Singulares 2020." J.J.G.-R. acknowledges support from the CAM/FEDER Project No. S2018/TCS-4342 (QUITEMAD-CM), CSIC Interdisciplinary Thematic Platform (PTI+) on Quantum Technologies (PTI-QTEP+). The construction of the facility was supported by the European Research Council (Contract No. 278648-TRAPSENSOR), Projects No. FPA2015-67694-P and No. FPA2012-32076; infrastructure Projects No. UNGR10-1E-501, No. UNGR13-1E-1830, and No. EQC2018-005130-P (MICINN/FEDER/UGR), and Grants No. IE-5713 and No. IE2017-5513 (Junta de Andalucía-FEDER).

APPENDIX A: QUANTUM DESCRIPTION OF THE DIFFERENT SUBSYSTEMS

The quantum Hamiltonians presented in Sec. III are deduced from considerations given in this Appendix.

1. Quantum description of the ion motion in a Penning trap

The quantum Hamiltonian of an ion in a Penning trap is given by [22]

$$H_{\text{ion}} = \frac{1}{2m_{\text{ion}}}\left(\hat{p}_x^2 + \hat{p}_y^2 + \hat{p}_z^2\right) + \frac{\omega_c}{2}(\hat{x}\hat{p}_y - \hat{y}\hat{p}_x) + \frac{1}{2}m_{\text{ion}}\frac{\omega_c^2 - 2\omega_z^2}{4}(\hat{x}^2 + \hat{y}^2) + \frac{1}{2}m_{\text{ion}}\omega_z^2\hat{z}^2 \quad \text{(A1)}$$

that can be rewritten in the form

$$H_{\text{ion}} = H_z + H_+ + H_- = \hbar\omega_z\left(a_z^\dagger a_z + \frac{1}{2}\right) + \hbar\omega_+\left(a_+^\dagger a_+ + \frac{1}{2}\right) - \hbar\omega_-\left(a_-^\dagger a_- + \frac{1}{2}\right), \quad \text{(A2)}$$

after defining the Fock creation and annihilation operators $a^\dagger$ and a, respectively, for each of the eigenmotions of the ion in the trap: modified cyclotron (+), magnetron (−), and axial

(z). These operators read

$$a_z = \sqrt{\frac{N_{\rm ion} m_{\rm ion}\omega_z}{2\hbar}}\left[\hat{z} + \frac{i}{m_{\rm ion}\omega_z}\hat{p}_z\right], \quad a_\pm = \sqrt{\frac{N_{\rm ion} m_{\rm ion}}{2\hbar(\omega_+ - \omega_-)}}\left[\left(\frac{\hat{p}_x}{m_{\rm ion}} - \omega_\pm \hat{y}\right) \pm i\left(\frac{\hat{p}_y}{m_{\rm ion}} + \omega_\pm \hat{x}\right)\right],$$
$$a_z^\dagger = \sqrt{\frac{N_{\rm ion} m_{\rm ion}\omega_z}{2\hbar}}\left[\hat{z} - \frac{i}{m_{\rm ion}\omega_z}\hat{p}_z\right], \quad a_\pm^\dagger = \sqrt{\frac{N_{\rm ion} m_{\rm ion}}{2\hbar(\omega_+ - \omega_-)}}\left[\left(\frac{\hat{p}_x}{m_{\rm ion}} - \omega_\pm \hat{y}\right) \mp i\left(\frac{\hat{p}_y}{m_{\rm ion}} + \omega_\pm \hat{x}\right)\right], \tag{A3}$$

where we have replaced the single ion with mass $m_{\rm ion}$, charge $q_{\rm ion}$, and momentum $(\hat{p}_x, \hat{p}_y, \hat{p}_z)$ by an ion cloud with $N_{\rm ion}$, considering them as a single ion with mass $N_{\rm ion}m_{\rm ion}$, charge $N_{\rm ion}q_{\rm ion}$, and momentum $N_{\rm ion}(\hat{p}_x, \hat{p}_y, \hat{p}_z)$.

2. Quantum description of a quartz crystal

In a similar way as it has been done for a single ion, the operators to describe the characteristic voltage and intensity in the crystal can be written as

$$\hat{V} \equiv \frac{\hat{Q}}{C_{\rm q}} = \frac{1}{k}\sqrt{\frac{\hbar}{2m_{\rm q}\omega_{\rm q}}}(b^\dagger + b) = \frac{V_0}{\sqrt{2}}(b^\dagger + b) \tag{A4}$$

and

$$\hat{I} = i\frac{C_{\rm q}}{k}\sqrt{\frac{\hbar\omega_{\rm q}}{2m_{\rm q}}}(b^\dagger - b). \tag{A5}$$

The expected values can be expressed as

$$\langle\hat{V}\rangle = \frac{1}{k}\sqrt{\frac{2\hbar}{m_{\rm q}\omega_{\rm q}}}{\rm Re}\{\langle b\rangle\}, \qquad \langle\hat{I}\rangle = \frac{C_{\rm q}}{k}\sqrt{\frac{2\hbar\omega_{\rm q}}{m_{\rm q}}}{\rm Im}\{\langle b\rangle\}. \tag{A6}$$

3. Quantum description of the interaction quartz ions

In order to model the interaction between the ions and the quartz we assume for the latter a charge $\hat{Q}' = \hat{Q} + \xi\hat{Q}_{\rm ion}$ and a current $\hat{I}' = \hat{I} + \xi\hat{I}_{\rm ion}$, where $\hat{Q}_{\rm ion}$ and $\hat{I}_{\rm ion}$ have been defined in Eqs. (5) and (6), respectively, and ξ is a positive number smaller than 1 to account for the effective ions' charge and current. $\hat{Q}$ and $\hat{I}$ are the charge and current associated to the quartz resonator, i.e., when there are no ions in the trap (or if they are not in resonance with the crystal). The Hamiltonian can be given as

$$\begin{aligned} H_{\rm q} + H_{\rm int} &= \left(\frac{k}{C_{\rm q}}\right)^2\left[\frac{m_{\rm q}(\hat{I} + \xi\hat{I}_{\rm ion})^2}{2} + \frac{m_{\rm q}\omega_{\rm q}^2(\hat{Q} + \xi\hat{Q}_{\rm ion})^2}{2}\right] \\ &= \left(\frac{k}{C_{\rm q}}\right)^2\left\{\frac{m_{\rm q}}{2}\left[\hat{I}^2 + \left(\frac{\xi N_{\rm ion}q_{\rm ion}\alpha}{2d_0 m_{\rm ion}}\right)^2\hat{p}_x^2 + \left(-\frac{\xi N_{\rm ion}q_{\rm ion}\alpha}{d_0 m_{\rm ion}}\right)\hat{I}\hat{p}_x\right] + \frac{m_{\rm q}\omega_{\rm q}^2}{2}\left[\hat{Q}^2 + \left(\frac{\xi N_{\rm ion}q_{\rm ion}\alpha}{2d_0}\right)^2\hat{x}^2\right.\right. \\ &\quad \left.\left. + \left(-\frac{\xi N_{\rm ion}q_{\rm ion}\alpha}{d_0}\right)\hat{Q}\hat{x} + (-\xi N_{\rm ion}q_{\rm ion}\alpha)\hat{Q} + \left(\frac{\xi^2 N_{\rm ion}^2 q_{\rm ion}^2\alpha^2}{2d_0}\right)\hat{x} + \left(\frac{\xi N_{\rm ion}q_{\rm ion}\alpha}{2}\right)^2\right]\right\}. \end{aligned} \tag{A7}$$

The term containing $\hat{x}^2$ will add a negligible amount $\Delta\omega_{\rm ion}$ to the observed ions' frequency; the term containing ${\hat{p}_x}^2$ will increase the weight of ${\hat{p}_x}^2$ in the Hamiltonian by a small amount ε; whereas the ones with $\hat{x}$ and $\hat{Q}$ will insignificantly shift the minimum of the potential well by $\hat{x}_0$ and $\hat{Q}_0$, respectively. Adding these terms to the Hamiltonians of ions in one direction and quartz [Eqs. (8) and (9)] and rearranging terms we obtain

$$\begin{aligned} H_{\rm q} + H_{{\rm ion},x} \sim{}& \left(\frac{k}{C_{\rm q}}\right)^2\frac{m_{\rm q}}{2}\left[\hat{I}^2 + \omega_{\rm q}^2(\hat{Q} - \hat{Q}_0)^2\right] \\ &+ \frac{N_{\rm ion}}{2}m_{\rm ion}(\omega_{\rm ion} + \Delta\omega_{\rm ion})^2(\hat{x} - \hat{x}_0)^2 \\ &+ \frac{N_{\rm ion}}{2m_{\rm ion}}(1 + \varepsilon){\hat{p}_x}^2, \end{aligned} \tag{A8}$$

where

$$\Delta\omega_{\rm ion} = \sqrt{\omega_{\rm ion}^2 + \frac{\hbar N_{\rm ion}\omega_{\rm q}}{m_{\rm ion}}\left(\frac{\xi q_{\rm ion}\alpha}{2C_{\rm q}V_0 d_0}\right)^2} - \omega_{\rm ion}, \tag{A9}$$

$$\varepsilon = \frac{\hbar N_{\rm ion}}{m_{\rm ion}\omega_{\rm q}}\left(\frac{\xi q_{\rm ion}\alpha}{2C_{\rm q}V_0 d_0}\right)^2, \tag{A10}$$

$$\hat{x}_0 = -\frac{\hbar N_{\rm ion}\omega_{\rm q}}{4d_0 m_{\rm ion}\omega_{\rm ion}^2}\left(\frac{\xi q_{\rm ion}\alpha}{C_{\rm q}V_0}\right)^2, \tag{A11}$$

and

$$\hat{Q}_0 = \tfrac{1}{2}\xi N_{\rm ion}q_{\rm ion}\alpha. \tag{A12}$$

In our experiment $\Delta\omega_{\rm ion} \leqslant 2\pi \times 10^{-5}$ Hz, $\varepsilon \leqslant 4 \times 10^{-12}$, $|\hat{x}_0| \leqslant 4 \times 10^{-14}$ m, and $\hat{Q}_0 \leqslant 1.1 \times 10^{-16}$ C.

APPENDIX B: PROOFS FOR THE COMPUTATION OF THE PSD

1. Driven quartz-ion dynamics

The basis of operators **A** almost satisfies the conditions for the quantum regression theorem [23]. First of all, their

expectation values evolve according to

$$\frac{d}{dt}\langle \mathbf{A}(t)\rangle = \mathrm{tr}\left\{\mathbf{A}(t)\frac{d}{dt}\rho\right\} = \mathrm{tr}\{\mathbf{A}(t)\mathcal{L}_{\mathrm{tot}}(\rho)\}. \tag{B1}$$

Using the explicit form of the Lindblad terms and the commutation relations between bosonic operators (e.g., Appendix B3), one may find a linear relation

$$\mathrm{tr}\{A_m\mathcal{L}_{\mathrm{tot}}(O)\} = -\sum_n M_{mn}\mathrm{tr}(A_n O) + F_m, \tag{B2}$$

valid for any operator O, in particular the density matrix (B1), where

$$M_{mn} = \begin{pmatrix} \mathbf{m} & 0 \\ 0 & \mathbf{m}^* \end{pmatrix}_{mn}, \text{ with } \mathbf{m} = \begin{pmatrix} \frac{\gamma_{\mathrm{ion}}}{2} + i\tilde{\omega}_{\mathrm{ion}} & ig^* \\ ig & \frac{\gamma_{\mathrm{q}}}{2} + i\tilde{\omega}_{\mathrm{q}} \end{pmatrix} \tag{B3}$$

is a block-diagonal matrix that represents the nondriven dynamics of the system and

$$F_m = \begin{pmatrix} f_{\mathrm{ion}}e^{-i\phi_{\mathrm{ion}}} \\ f_{\mathrm{q}}e^{-i\phi_{\mathrm{q}}} \\ f_{\mathrm{ion}}e^{i\phi_{\mathrm{ion}}} \\ f_{\mathrm{q}}e^{i\phi_{\mathrm{q}}} \end{pmatrix}_m \tag{B4}$$

is the force term, which is constant because of the rotating frame. This equation allows us to write dynamical equations for the first-order moments:

$$\frac{d}{dt}\langle \mathbf{A}(t)\rangle = -\mathbf{M}\langle \mathbf{A}(t)\rangle + \mathbf{F}, \tag{B5}$$

which for $a(t)$ and $b(t)$ can be written as

$$\begin{aligned} \frac{d}{dt}\langle a(t)\rangle &= -\left(\frac{\gamma_{\mathrm{ion}}}{2} + i\tilde{\omega}_{\mathrm{ion}}\right)\langle a\rangle - ig^*\langle b\rangle - if_{\mathrm{ion}}e^{-i\phi_{\mathrm{ion}}}, \\ \frac{d}{dt}\langle b(t)\rangle &= -ig\langle a\rangle - \left(\frac{\gamma_{\mathrm{q}}}{2} + i\tilde{\omega}_{\mathrm{q}}\right)\langle b\rangle - if_{\mathrm{q}}e^{-i\phi_{\mathrm{q}}}. \end{aligned} \tag{B6}$$

If one defines the displaced operators

$$\mathbf{A}^0 := \mathbf{A} - \mathbf{A}_{\mathbf{F}}, \text{ with } \mathbf{A}_{\mathbf{F}} := \mathbf{M}^{-1}\mathbf{F}, \tag{B7}$$

they do satisfy a linear differential equation without source term, which is the requirement for the quantum regression theorem:

$$\frac{d}{dt}\langle \mathbf{A}^0(t)\rangle = -\mathbf{M}\langle \mathbf{A}^0(t)\rangle. \tag{B8}$$

The dynamics of the quartz-ion system can be solved by assuming that the force is switched on at time t_s and the driving continues until time t:

$$\begin{aligned} \langle \mathbf{A}^0(t)\rangle &= \mathbf{U}(t-t_s)\langle \mathbf{A}^0(t_s)\rangle, \\ \langle \mathbf{A}(t)\rangle &= e^{-\mathbf{M}(t-t_s)}\langle \mathbf{A}(t_s)\rangle + (\mathbb{1} - e^{-\mathbf{M}(t-t_s)})\mathbf{A}_{\mathbf{F}}, \end{aligned} \tag{B9}$$

using the 4×4 contractive matrix $\mathbf{U}(t) = \exp(-\mathbf{M}t)$. In the limit $t\to+\infty$ this dynamics brings the ion and quartz to a unique stationary solution:

$$\lim_{t\to+\infty}\langle \mathbf{A}(t)\rangle = \mathbf{M}^{-1}\mathbf{F} = \mathbf{A}_{\mathbf{F}}. \tag{B10}$$

The asymptotic state of the driving $\mathbf{A}_{\mathbf{F}}$ depends on the inverse of the matrix $\mathbf{M} = \mathbf{M}(\omega_{\mathrm{rf}})$, which itself depends on the detunings between the drive and the ions and quartz frequencies $\omega_{\mathrm{ion}} - \omega_{\mathrm{rf}}$ and $\omega_{\mathrm{q}} - \omega_{\mathrm{rf}}$. This produces the usual Lorentzian profile of $\mathbf{A}_{\mathbf{F}}$ as a function of ω.

In the experiment, the driving is stopped at a time $t = 0$. The dynamics of the ion and the quartz naturally revert to the dissipation-induced friction, and the displacements of the Fock operators (and the average values of voltage and intensity) naturally revert back to zero:

$$\langle \mathbf{A}(t)\rangle = \mathbf{U}(t)\mathbf{A}_{\mathbf{F}} \to 0, \text{ as } t\to\infty. \tag{B11}$$

The study of two-time correlators requires higher-order moments of the quartz-ion system. With similar effort, a linear differential equation for the same-time correlators $\langle A_m(t)A_n(t)\rangle$ can be computed:

$$\begin{aligned} \frac{d}{dt}\langle A_nA_m\rangle = &-\sum_r M_{mr}\langle A_rA_n\rangle + F_m\langle A_n\rangle \\ &-\sum_r M_{ns}\langle A_mA_s\rangle + \langle A_m\rangle F_n + C_{mn}, \end{aligned} \tag{B12}$$

with a real matrix C_{nm} (see Appendix B3). This equation has a unique stationary state satisfying

$$\sum_r M_{mr}\langle A_r^0A_n^0\rangle + \sum_s M_{ns}\langle A_m^0A_s^0\rangle + C_{mn} = 0. \tag{B13}$$

The solution to Eq. (B13) is the correlation matrix of a thermal state, dictated by the n_{ion} and n_{q} occupations that define C_{mn}. This means that the stationary solution during the driving can be written as two contributions: a thermal state and a displacement induced by the driving:

$$\langle A_nA_m\rangle = \langle A_nA_m\rangle_{\mathrm{th}} + \langle A_F\rangle_m\langle A_F\rangle_n. \tag{B14}$$

After stopping the driving at $t = 0$, the dynamics of the same-time correlator follows a similar route as the first-order moment, with a constant term, given by the thermal fluctuations, and a product of two displacements:

$$\langle A_n(t)A_m(t)\rangle = \langle A_nA_m\rangle_{\mathrm{th}} + \langle A_m(t)\rangle\langle A_n(t)\rangle, \tag{B15}$$

which attenuate as described above in Eq. (B11).

2. Free dynamics of two-time correlators

Once the driving stops, the $\mathbf{A}$ operators satisfy a differential equation without source term that can be solved linearly:

$$\langle \mathbf{A}(t)\rangle = \mathbf{U}(t-t_0)\langle \mathbf{A}(t_0)\rangle;\ t, t_0 > 0. \tag{B16}$$

This allows using the quantum regression theorem to derive two-time correlators at all possible orderings of time $t, \tau > 0$

after switching off the driving:

$$\langle A_m(t+\tau)A_n(t)\rangle = \sum_r U_{mr}(\tau)\,\langle A_r(t)A_n(t)\rangle \tag{B17}$$

and

$$\langle A_m(t)A_n(t+\tau)\rangle = \sum_r U_{nr}(\tau)\,\langle A_m(t)A_r(t)\rangle\,. \tag{B18}$$

Given the simple structure of the same-time correlator (B15), we can derive an explicit formula for the two-time correlator we use in the PSD. This formula has a simple contribution given by the global displacement, and a slightly more complex one given by the thermal fluctuations:

$$\langle A_m(t_2)A_n(t_1)\rangle = \langle A_m(t_2)\rangle\,\langle A_n(t_1)\rangle + \sum_r \begin{cases} U_{mr}(t_2-t_1)\,\langle A_rA_n\rangle_{\rm th} & \text{if } t_2 > t_1, \\ U_{nr}(t_1-t_2)\,\langle A_mA_r\rangle_{\rm th} & \text{else.} \end{cases} \tag{B19}$$

3. Same-time correlator equations

The dynamics of the correlator matrix $\langle A_m(t)A_n(t)\rangle$ does not follow exactly the quantum regression theorem [23]. The equation

$$\begin{aligned}
&{\rm tr}\{A_mA_n\mathcal{L}_{\rm tot}(O)\} \\
&\quad = -\frac{i}{\hbar}{\rm tr}\{[A_mA_n,H],O\} \\
&\qquad + \frac{\gamma_{\rm q}}{2}n_{\rm q}{\rm tr}\{b[A_mA_n,b^\dagger]O + [b,A_mA_n]b^\dagger O\} \\
&\qquad + \frac{\gamma_{\rm q}}{2}(n_{\rm q}+1){\rm tr}\{b^\dagger[A_mA_n,b]O + [b^\dagger,A_mA_n]bO\} \\
&\qquad + \frac{\gamma_{\rm ion}}{2}n_{\rm ion}{\rm tr}\{a[A_mA_n,a^\dagger]O + [a,A_mA_n]a^\dagger O\} \\
&\qquad + \frac{\gamma_{\rm ion}}{2}(n_{\rm ion}+1){\rm tr}\{a^\dagger[A_mA_n,a]O + [a^\dagger,A_mA_n]aO\}
\end{aligned} \tag{B20}$$

transforms into

$$\begin{aligned}
{\rm tr}\{A_nA_m\mathcal{L}_{\rm tot}(O)\} = &-\sum_r M_{mr}\,\langle A_rA_n\rangle + F_m\,\langle A_n\rangle \\
&-\sum_s M_{ns}\,\langle A_mA_s\rangle + \langle A_m\rangle\,F_n \\
&+ C_{mn}.
\end{aligned} \tag{B21}$$

The real matrix $\mathbf{C}$ is defined as

$$\begin{aligned}
C_{mn} = &\,\gamma_{\rm q}(n_{\rm q}[b,A_m][A_n,b^\dagger] + (n_{\rm q}+1)[b^\dagger,A_m][A_n,b]) \\
&+ \gamma_{\rm ion}(n_{\rm ion}[a,A_m][A_n,a^\dagger] \\
&+ (n_{\rm ion}+1)[a^\dagger,A_m][A_n,a]),
\end{aligned} \tag{B22}$$

which evaluates to

$$\begin{aligned}
\mathbf{C} &= \begin{pmatrix} 0 & 0 & \gamma_{\rm ion}(n_{\rm ion}+1) & 0 \\ 0 & 0 & 0 & \gamma_{\rm q}(n_{\rm q}+1) \\ \gamma_{\rm ion}n_{\rm ion} & 0 & 0 & 0 \\ 0 & \gamma_{\rm q}n_{\rm q} & 0 & 0 \end{pmatrix} \\
&= \begin{pmatrix} 0 & \gamma(\mathbf{n}+\mathbb{1}) \\ \gamma\mathbf{n} & 0 \end{pmatrix}.
\end{aligned} \tag{B23}$$

4. Fourier-space propagator

The Fourier transforms of the first-order moments $\tilde{\mathbf{A}}$ are related to the initial values of the first-order moments at t_0 via a propagator

$$\tilde{\mathbf{A}}(\omega;t_0,t_1) = \frac{1}{\sqrt{t_1-t_0}}\mathbf{W}(-\omega,t_1-t_0)\,\langle\mathbf{A}(t_0)\rangle\,, \tag{B24}$$

where we have introduced the Green's function

$$\begin{aligned}
\mathbf{W}(\pm\omega,t_d) &:= \int_0^{t_d} e^{-\mathbf{M}\tau}e^{\pm i\omega\tau}d\tau \\
&= (\pm i\omega - \mathbf{M})^{-1}\left(e^{(\pm i\omega-\mathbf{M})t_d} - \mathbb{1}\right).
\end{aligned} \tag{B25}$$

The Lorentzian prefactor to the exponential can be computed as the inverse of two 2×2 matrices:

$$(i\omega-\mathbf{M})^{-1} = \begin{pmatrix} (i\omega-\mathbf{m})^{-1} & 0 \\ 0 & (i\omega-\mathbf{m}^*)^{-1} \end{pmatrix}, \tag{B26}$$

for positive and negative values of ω. This equation can be written in terms of the Lorentzian envelope (36) and the matrix

$$\mathbf{G}(\omega) = \begin{pmatrix} -\frac{\gamma_{\rm q}}{2} + i(\omega-\tilde{\omega}_{\rm q}) & ig \\ ig^* & -\frac{\gamma_{\rm ion}}{2} + i(\omega-\tilde{\omega}_{\rm ion}) \end{pmatrix}, \tag{B27}$$

resulting in

$$(i\omega-\mathbf{M})^{-1} = \begin{pmatrix} F(\omega)\mathbf{G}(\omega) & 0 \\ 0 & F(-\omega)^*\mathbf{G}(-\omega)^* \end{pmatrix}. \tag{B28}$$

Note that $F(\omega)\simeq 0$ whenever $\omega<0$, so that certain parts of the inverse $(\pm i\omega+\mathbf{M})^{-1}$ can be neglected depending on whether we choose the positive or negative sign accompanying ω.

5. PSD simplifications

It is convenient to separate the PSD integral into two components, taking into account the ordering of time:

$$\begin{aligned}
S^{\rm th}_{mn}(\omega) = &\frac{1}{t_d}\int_{t_0}^{t_1}d\tau_1\int_{t_0}^{\tau_1}d\tau_2 e^{i\omega(\tau_1-\tau_2)}\,\langle A_m(\tau_2)A_n(\tau_1)\rangle \\
&+ \frac{1}{t_d}\int_{t_0}^{t_1}d\tau_1\int_{\tau_1}^{t_1}d\tau_2 e^{i\omega(\tau_1-\tau_2)}\,\langle A_m(\tau_2)A_n(\tau_1)\rangle\,.
\end{aligned} \tag{B29}$$

The integration limits can be reordered to bring out the lowest time

$$\begin{aligned}
S^{\rm th}_{mn}(\omega) = &\frac{1}{t_d}\int_{t_0}^{t_1}d\tau_2\int_{\tau_2}^{t_1}d\tau_1 e^{i\omega(\tau_1-\tau_2)}\,\langle A_m(\tau_2)A_n(\tau_1)\rangle \\
&+ \frac{1}{t_d}\int_{t_0}^{t_1}d\tau_1\int_{\tau_1}^{t_1}d\tau_2 e^{i\omega(\tau_1-\tau_2)}\,\langle A_m(\tau_2)A_n(\tau_1)\rangle\,,
\end{aligned} \tag{B30}$$

and relabeled adequately:

$$\begin{aligned}
S^{\rm th}_{mn}(\omega) = &\frac{1}{t_d}\int_{t_0}^{t_1}dt\int_0^{t_d-t}d\tau e^{i\omega\tau}\,\langle A_m(t)A_n(t+s)\rangle \\
&+ \frac{1}{t_d}\int_{t_0}^{t_1}dt\int_0^{t_d-t}d\tau e^{-i\omega\tau}\,\langle A_m(t+s)A_n(t)\rangle\,.
\end{aligned} \tag{B31}$$

The first integral can be manipulated, noting that

$$\langle A_m(t)A_n(t+s)\rangle = \langle A_n(t+s)^\dagger A_m(t)^\dagger\rangle^* = \sum_{u,v} P_{nu}\,\langle A_u(t+s)A_v(t)\rangle^*\,P_{mv}, \quad \text{(B32)}$$

with some permutation matrices $\mathbf{P}$:

$$\mathbf{PA} = \mathbf{A}^\dagger. \quad \text{(B33)}$$

By doing so, one arrives at a single computation:

$$\mathbf{S}(\omega) = \mathbf{S}^+(\omega) + \mathbf{P}\mathbf{S}^+(\omega)^\dagger\mathbf{P}, \text{ with}$$

$$S^+_{mn}(\omega) = \frac{1}{t_d}\int_{t_0}^{t_1} dt \int_0^{t_d-t} d\tau e^{-i\omega\tau}\,\langle A_m(t+s)A_n(t)\rangle\,.$$

In the particular case of computing the autocorrelation function of the voltage, $\mathbf{Pv} = \mathbf{v}$, we have

$$S(\omega) = 2\mathrm{Re}(\mathbf{v}^\mathrm{T}\mathbf{S}^+(\omega)\mathbf{v}). \quad \text{(B34)}$$

6. Thermal state

The thermal state's correlation matrix $T_{nm} = \langle A_n A_m\rangle_\mathrm{th}$ reads

$$\mathbf{T} = \begin{pmatrix} \langle a^2\rangle & \langle ab\rangle & \langle aa^\dagger\rangle & \langle ab^\dagger\rangle \\ \langle ba\rangle & \langle bb\rangle & \langle ba^\dagger\rangle & \langle bb^\dagger\rangle \\ \langle a^\dagger a\rangle & \langle a^\dagger b\rangle & \langle a^\dagger a^\dagger\rangle & \langle a^\dagger b^\dagger\rangle \\ \langle b^\dagger a\rangle & \langle b^\dagger b\rangle & \langle b^\dagger a^\dagger\rangle & \langle b^\dagger b^\dagger\rangle \end{pmatrix}_\mathrm{th}. \quad \text{(B35)}$$

It has a simple structure

$$\mathbf{T} = \begin{pmatrix} 0 & \mathbf{t}_{-\dagger} \\ \mathbf{t}_{\dagger-} & 0 \end{pmatrix}, \text{ with } \mathbf{t}_{-\dagger} = \mathbf{t}_{\dagger-} + \mathbb{1}, \quad \text{(B36)}$$

and satisfies the stationary equation

$$\mathbf{MT} + \mathbf{TM}^\mathrm{T} = \mathbf{C}, \quad \text{(B37)}$$

which gives the two equivalent conditions

$$\mathbf{m}\mathbf{t}_{-\dagger} + \mathbf{t}_{-\dagger}\mathbf{m}^\dagger = \gamma(\mathbf{n} + \mathbb{1}), \quad \text{(B38)}$$

$$\mathbf{m}^*\mathbf{t}_{\dagger-} + \mathbf{t}_{\dagger-}\mathbf{m}^\mathrm{T} = \gamma\mathbf{n}. \quad \text{(B39)}$$

The exact solution of these equations is given by

$$\langle b^\dagger b\rangle_\mathrm{th} = n_\mathrm{q} + \frac{4|g|^2(n_\mathrm{ion}-n_\mathrm{q})\gamma_\mathrm{ion}\Gamma_+}{4|g|^2\Gamma_+^2 + \gamma_\mathrm{ion}\gamma_\mathrm{q}(\Gamma_+^2 + 4\Omega_-^2)}, \quad \text{(B40)}$$

$$\langle a^\dagger b\rangle_\mathrm{th} = -\frac{2ig(n_\mathrm{ion}-n_\mathrm{q})(\Gamma_+ + 2i\Omega_+)}{4|g|^2\Gamma_+^2 + \gamma_\mathrm{ion}\gamma_\mathrm{q}(\Gamma_+^2 + 4\Omega_-^2)}, \quad \text{(B41)}$$

$$\langle a^\dagger a\rangle_\mathrm{th} = n_\mathrm{ion} - \frac{4|g|^2(n_\mathrm{ion}-n_\mathrm{q})\gamma_\mathrm{q}\Gamma_+}{4|g|^2\Gamma_+^2 + \gamma_\mathrm{ion}\gamma_\mathrm{q}(\Gamma_+^2 + 4\Omega_-^2)}, \quad \text{(B42)}$$

with the quantities $\Gamma_\pm := \gamma_\mathrm{ion} \pm \gamma_\mathrm{q}$ and $\Omega_\pm := \omega_\mathrm{ion} \pm \omega_\mathrm{q}$.

APPENDIX C: OTHER QUANTITIES FROM THE FIT

The omitted step of the fitting procedure described in the main text will be presented in this section [24]. In order to gradually reduce the number of free parameters and considering the signal with and without ions, the coupling constant $|g|$ has been obtained. The PSD near ν_+ continuously decreases after $t_0 \gtrsim 50$ ms as observed in Fig. 8, when the quartz crystal

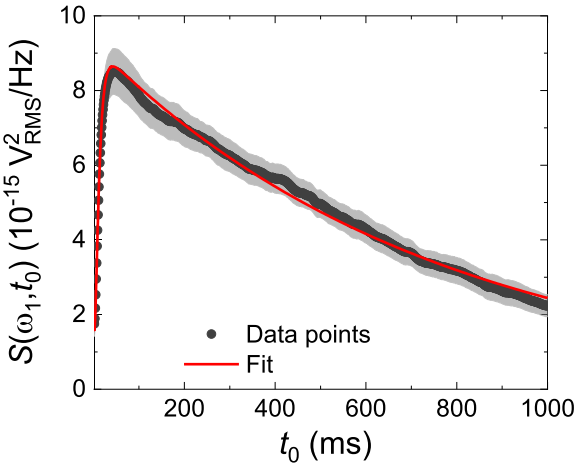

FIG. 8. $S(\omega, t_0)$ for a fixed frequency ω_1.

amplitude $\langle b(t_0)\rangle$ is already approximately zero (right panel of Fig. 9). This happens because the ion cloud is losing energy after $t_0 \gtrsim 50$ ms due to two main interactions: (1) with the quartz—ruled by the coupling constant $|g|$, the quartz absorbs energy from the cloud and dissipates it in a (relatively short) time $\approx 1/\gamma_\mathrm{q}$—and (2) with the thermal bath of the ions, ruled by the dissipative constant γ_ion.

The parameters $|g|$ and γ_ion play a similar role in the ions' energy. It is hard to distinguish them from fits and to get a stable parameter evolution. Therefore, γ_ion has been set to zero in all fits to simplify the analysis. Note that we have also let γ_ion be a free parameter for fits in the preliminary phase of the analysis. Its value was not stable with the evolution of t_0, although it was always several orders of magnitude lower than the bound given below [Eq. (C2)]. The other free parameters had values almost identical to the ones presented in the main text. $\gamma_\mathrm{ion} = 0$ is also justified for the very low value of γ_ion that we can estimate from other experiments with the same setup using ions generated outside the trap [25]. We also neglect, on the time scale of the experiment, the effect of ion-ion interactions and of induced image charges on the ions' center-of-mass motion, following

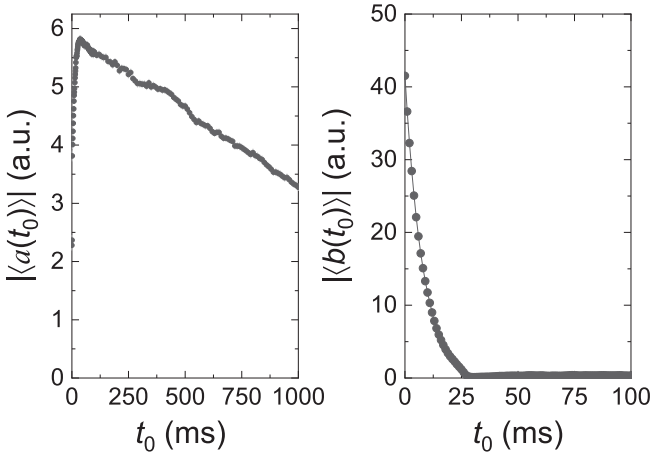

FIG. 9. Time evolution of $|\langle a(t_0)\rangle|$ and $|\langle b(t_0)\rangle|$.

the criteria of Ref. [14]. The value of $|g|$ has been obtained from a fit of the time evolution of the PSD at a single frequency value $\nu_1 = \nu_{\rm rf} + 1.35\,{\rm Hz}$ (Fig. 8), which is almost at the peak maximum for signals with large t_0. The theoretical shape of this evolution is governed by Eq. (29) but fixing several parameters (1) obtained from the fits of the signals without ions—$S^{\rm noise} = 3.101(5) \times 10^{-18}\, V_{\rm RMS}^2/{\rm Hz}$, $\nu_{\rm q}(t_0 = 0\,{\rm ms}) = \nu_{\rm rf} + 1.99(2)\,{\rm Hz}$, and $\gamma_{\rm q}(t_0 = 0\,{\rm ms})/2\pi = 39.81(4)$ Hz—and (2) by solving Eq. (B5) analytically—$\langle a(t)\rangle$, $\langle a^\dagger(t)\rangle$, $\langle b(t)\rangle$, and $\langle b^\dagger(t)\rangle$ at $t = t_1$—from its values at $t = t_0$. Figure 9 shows the evolution of $|\langle a(t_0)\rangle|$ and $|\langle b(t_0)\rangle|$ as a function of t_0.

Considering these values, Eq. (29) is now a function of the independent variable t_0 and the free-fit parameters $|\langle a(t_0 = 0)\rangle|$, $|\langle b(t_0 = 0)\rangle|$, $|g|$, and the relative phase $\delta(t_0 = 0)$. Since $\gamma_{\rm ion} = 0$, the value $|g| = 2\pi \times 1.449(2)\,{\rm Hz}$ is an upper limit. We have computed a second-order Taylor expansion around the time $t_{\rm peak} \approx 50$ ms given by

$$S(\omega_1, t_0) \approx S^{\rm th}(\omega_1) + S^{\rm noise} + \frac{V_0^2}{2t_{\rm d}}\left(\frac{|g|\langle a^\dagger(t_{\rm peak})\rangle}{|g|^2 + \gamma_{\rm ion}\gamma_{\rm q}/4}\right)^2 \times [1 - 2\gamma_{\rm ion}\Delta t - (|g|^2 - \gamma_{\rm ion}\gamma_{\rm q}/4)\Delta t^2 + \mathcal{O}(\Delta t^3)], \tag{C1}$$

to loosely quantify the magnitude of a $\gamma_{\rm ion}$ discernible from $|g|$. $\Delta t \equiv t_0 - t_{\rm peak}$ and we assume $\omega = \omega_{\rm ion} \approx \omega_{\rm q}$, $\gamma_{\rm q} \gg \gamma_{\rm ion}$, and $\langle b^\dagger(t_{\rm peak})\rangle \approx 0$. In this context, we can consider $\gamma_{\rm ion}$ small if the quadratic term is not negligible, i.e.,

$$\gamma_{\rm ion} < 4\frac{|g|^2}{\gamma_{\rm q}} \approx 2\pi \times 0.2\ {\rm Hz}. \tag{C2}$$

[1] E. G. Myers, Atoms **7**, 37 (2019).

[2] M. Borchert, J. Devlin, S. Erlewein, M. Fleck, J. Harrington, T. Higuchi, B. Latacz, F. Voelksen, E. Wursten, F. Abbass, M. Bohman, A. Mooser, D. Popper, M. Wiesinger, C. Will, K. Blaum, Y. Matsuda, C. Ospelkaus, W. Quint, J. Walz *et al.*, Nature (London) **601**, 53 (2022).

[3] C. L. Hendrickson, J. P. Quinn, N. K. Kaiser, D. F. Smith, G. T. Blakney, T. Chen, A. G. Marshall, C. R. Weisbrod, and S. C. Beu, J. Am. Soc. Mass Spectrom. **26**, 1626 (2015).

[4] A. Rischka, H. Cakir, M. Door, P. Filianin, Z. Harman, W. J. Huang, P. Indelicato, C. H. Keitel, C. M. König, K. Kromer, M. Müller, Y. N. Novikov, R. X. Schüssler, C. Schweiger, S. Eliseev, and K. Blaum, Phys. Rev. Lett. **124**, 113001 (2020).

[5] S. Rainville, J. K. Thompson, and D. E. Pritchard, Science **303**, 334 (2004).

[6] R. M. Weisskoff, G. P. Lafyatis, K. R. Boyce, E. A. Cornell, R. W. Flanagan, and D. Pritchard, J. Appl. Phys. **63**, 4599 (1988).

[7] S. Ulmer, H. Kracke, K. Blaum, S. Kreim, A. Mooser, W. Quint, C. C. Rodegheri, and J. Walz, Rev. Sci. Instrum. **80**, 123302 (2009).

[8] S. Lohse, J. Berrocal, M. Block, S. Chemarev, J. M. Cornejo, J. G. Ramírez, and D. Rodríguez, Rev. Sci. Instrum. **90**, 063202 (2019).

[9] S. Lohse, J. Berrocal, S. Böhland, J. van de Laar, M. Block, S. Chemarev, C. E. Düllman, S. Nagy, J. G. Ramírez, and D. Rodríguez, Rev. Sci. Instrum. **91**, 093202 (2020).

[10] J. Berrocal, S. Lohse, F. Domínguez, M. J. Gutiérrez, F. J. Fernández, M. Block, J. J. García-Ripoll, and D. Rodríguez, Quantum Sci. Technol. **6**, 044002 (2021).

[11] M. Block, D. Ackermann, K. Blaum, C. Droese, M. Dworschak, S. Eliseev, T. Fleckenstein, E. Haettner, F. Herfurth, F. P. Heßberger, S. Hofmann, J. Ketelaer, J. Ketter, H.-J. Kluge, G. Marx, M. Mazzocco, Y. N. Novikov, W. R. Plaß, A. Popeko, S. Rahaman *et al.*, Nature (London) **463**, 785 (2010).

[12] E. Minaya Ramirez, D. Ackermann, K. Blaum, M. Block, C. Droese, Ch. E. Düllmann, M. Dworschak, M. Eibach, S. Eliseev, E. Haettner, F. Herfurth, F. P. Heßberger, S. Hofmann, J. Ketelaer, G. Marx, M. Mazzocco, D. Nesterenko, Yu. N. Novikov, W. R. Plaß, D. Rodríguez *et al.*, Science **337**, 1207 (2012).

[13] D. Rodríguez, K. Blaum, W. Nörtershäuser, M. Ahammed, A. Algora, G. Audi, J. Äystö, D. Beck, M. Bender, J. Billowes, M. Block, C. Böhm, G. Bollen, M. Brodeur, T. Brunner, B. A. Bushaw, R. B. Cakirli, P. Campbell, D. Cano-Ott, G. Cortés *et al.*, Eur. Phys. J. Spec. Top. **183**, 1 (2010).

[14] D. J. Wineland and H. G. Dehmelt, J. Appl. Phys. **46**, 919 (1975).

[15] S. Sturm, I. Arapoglou, A. Egl, M. Höcker, S. Kraemer, T. Sailer, B. Tu, A. Weigel, R. Wolf, J. C. López-Urrutia, and K. Blaum, Eur. Phys. J. Spec. Top. **227**, 1425 (2019).

[16] D. J. Heinzen and D. J. Wineland, Phys. Rev. A **42**, 2977 (1990).

[17] D. Rodríguez, Appl. Phys. B **107**, 1031 (2012).

[18] M. Bohman, V. Grunhofer, C. Smorra, M. Wiesinger, C. Will, M. J. Borchert, J. A. Devlin, S. Erlewein, M. Fleck, S. Gavranovic, J. Harrington, B. Latacz, A. Mooser, D. Popper, E. Wursten, K. Blaum, Y. Matsuda, C. Ospelkaus, W. Quint, J. Walz *et al.*, Nature (London) **596**, 514 (2021).

[19] S. Kotler, R. W. Simmonds, D. Leibfried, and D. J. Wineland, Phys. Rev. A **95**, 022327 (2017).

[20] L. S. Brown and G. Gabrielse, Rev. Mod. Phys. **58**, 233 (1986).

[21] A. A. Clerk, M. H. Devoret, S. M. Girvin, F. Marquardt, and R. J. Schoelkopf, Rev. Mod. Phys. **82**, 1155 (2010).

[22] F. Crimin, B. M. Garraway, and J. Verdú, J. Mod. Opt. **65**, 427 (2018).

[23] H.-P. Breuer and F. Petruccione, *The Theory of Open Quantum Systems* (Oxford University, New York, 2010).

[24] E. Altozano, Estudio de resonadores de cuarzo para experimentos con trampas Penning, Master's thesis, Universidad de Granada, 2021.

[25] J. Berrocal, E. Altozano, F. Domínguez, M. J. Gutiérrez, J. Cerrillo, F. J. Fernández, M. Block, C. Ospelkaus, and D. Rodríguez, Phys. Rev. A **105**, 052603 (2022).